Available online at www.sciencedirect.com
ScienceDirect
Journal of Nuclear Materials 361 (2007) 69–77
journal of nuclear materials
www.elsevier.com/locate/jnucmat

Elastic and electronic properties and stability of $SrThO_3$, $SrZrO_3$ and ThO_2 from first principles

I.R. Shein, K.I. Shein, A.L. Ivanovskii *

Institute of Solid State Chemistry, Ural Branch of the Russian Academy of Sciences, 620041 Ekaterinburg, Russia

Received 13 September 2006; accepted 17 November 2006

Abstract

First-principle calculations in the framework of the full-potential linearized-augmented-plane-wave method (FLAPW, as implemented into the WIEN-2k code) have been performed to understand the structural, elastic, cohesive and electronic properties of the meta-stable cubic strontium thorate $SrThO_3$. The optimized lattice parameters, elastic parameters, formation energies, densities of states, band structures and charge density distributions are obtained and discussed in comparison with those of cubic $SrZrO_3$ and ThO_2.

1. Introduction

Thorium-based nuclear fuels are of great interest for the future nuclear industry. For example, it is proposed to use a ThO_2 matrix with admixtures of uranium and plutonium oxides as advanced fuel materials for the thermal breeder reactors and high-temperature gas cooled reactors. In this context, the presence of low-density phases such as ternary oxides M_2ThO_3 or $MThO_3$ forming due to the interaction of the fission products (M = Rb, Ba, Sr, etc.) with thoria, may critically affect the properties of the fuel such as thermal expansion, conductivity, and can be also responsible for the swelling of the fuel pins, see [1–3].

Since strontium is among the predominant fission products, the properties of the perovskite-like strontium thorate ($SrThO_3$) caused a lot of interest during the last decade [1–5]. Furthermore, the perovskite-type multi-component oxides of actinides are interesting candidates for hydrogen sensors, hydrogen gas separators, and are useful materials for many other electrochemical applications because of the unusual combination of their electronic and transport properties [6].

For the first time the synthesis of $SrThO_3$ by a conventional solid state route was reported in 1947 by Mary-Szabo [7]. More recently, Subasri et al. [5] noted the very limited solubility of SrO in thoria, and the formation of the single ternary phase is not achieved. On other hand, $SrThO_3$ samples are successfully prepared by a sol–gel method through the gel combustion technique [2–4].

The stability of $SrThO_3$ phase was discussed [3,4], using experimentally derived and calculated

* Corresponding author. Tel.: +7 343 3755331; fax: +7 373 3744495.
E-mail address: ivanovskii@ihim.uran.ru (A.L. Ivanovskii).

0022-3115/$ - see front matter © 2006 Elsevier B.V. All rights reserved.
doi:10.1016/j.jnucmat.2006.11.003

thermodynamic properties. The values of the Gibbs energy formation of $SrThO_3$ reveal that this compound is meta-stable in comparison with its constituent oxides (SrO and thoria), and as a consequence, there are difficulties to synthesize single phase strontium thorate. Among the other $SrThO_3$ properties, up to now only the structural data [1,2,8] and the linear thermal expansion coefficients [1] are reported. A qualitative explanation of the relative stability of perovskites $SrMO_3$ (in particular, for M^{4+} ions) has been made [4] in terms of Goldschmidt's tolerance factor t [9], which represents the size effect by means of the packing of spherical ions. It is based on ionic radii i.e. purely ionic bonding is assumed. For the stable $SrMO_3$ phases, the t-factor lies between 1.0 and 0.8 (for example, for $SrZrO_3$ $t = 0.861$), whereas for $SrThO_3$ the tolerance factor is about 0.780, i.e. this compound is placed on the border of the area of structural stability of perovskites, see for example reviews [10,11].

However, today any data concerning the electronic and cohesion properties and chemical bonding in $SrThO_3$ are absent, and the available attempts to explain the stability of this compound at the atomistic level are based on oversimplified models [4]. It is well known, that the first-principle calculations based on the density-functional theory (DFT) are an effective tool for the understanding and predicting of the various properties of the family of perovskites at the electronic level.

In this work to get better insight in the nature of this material the first-principle density-functional theory calculations using the full-potential linearized-augmented-plane-wave (FLAPW) method have been performed. Here we concentrate on the peculiarities of the elastic, cohesive and electronic properties of $SrThO_3$ (in assumption of cubic phase) – in comparison with thoria and the isoelectronic Sr zirconate $SrZrO_3$ (Zr^{4+}). Note that $SrZrO_3$ is also suitable for use in high-temperature applications such as fuel cells, steam electrolysis, and hydrogen gas sensors [12–14].

For $SrThO_3$, in result, the elastic constants (C_{ij}) are predicted and analyzed in comparison with those for ThO_2 and $SrZrO_2$. We employed the Voigt–Reuss–Hill (VRH) method to evaluate elastic parameters for these polycrystalline materials from C_{ij} of single crystals. In this way for the first time, the main elastic parameters for polycrystalline $SrThO_3$, ThO_2 and $SrZrO_2$: bulk modulus (B_0), compressibility (β), shear modulus (G), Young modulus (Y), Poisson ratio (ν), Lame constants (λ, μ) are predicted and analyzed. Next, using total energy calculations, the heats of formation of the mentioned Th, Zr-based perovskites (in assumption of formal reactions: $SrThO_3 \leftrightarrow SrO + ThO_2$ and $SrZrO_3 \leftrightarrow SrO + ZrO_2$) were estimated and discussed. The electronic bands and densities of states for ThO_2, $SrThO_2$ and $SrZrO_2$ have been obtained by study of their electronic properties. Finally, we assess the oxygen $K\alpha$ X-ray emission spectra (XES; O: $2p \leftrightarrow s$ transitions) for ThO_2 and $SrThO_3$ – for discussion of the applicability of this method for the characterizations of these systems.

2. Models and method

Perovskite $SrThO_3$ is reported in JCPDS data [8] to have a pseudo-monoclinic unit cell with $a = b = c = 0.884$ nm and $\beta = 90°$, whereas according to Purohit et al. [1] $SrThO_3$ was monoclinic with lattice parameters $a = 0.6319$; $b = 0.3240$; $c = 0.4928$ nm and $\beta = 117.38°$.

On the first stage, the considered $SrMO_3$ perovskites (here M = Th and Zr) are assumed to have ideal cubic structure (s.g. 221) where atomic positions in the elementary cell are M: 1a (0,0 0); I: 3d (0, 0, 1/2,); and Sr: 1b (1/2, 1/2, 1/2). Thoria adopts also cubic (fluorite-like) structure; the atomic positions in the elementary cell are Th: (0, 0, 0) and oxygen: (1/4, 1/4, 1/4). The electronic configurations are taken $[Kr]4d^25s^2$ for Zr, $[Rn]6d^27s^2$ for Th, $[Kr]5s^2$ for Sr and $[He]2s^22p^4$ for O. Here, the noble gas cores are distinguished from the sub-shells of valence electrons.

The band-structure calculations of the all mentioned compounds were done in the framework of the full potential all-electron method with the mixed basis APW+lo (LAPW) method implemented in the WIEN2k suite of programs [15]. The generalized gradient correction (GGA) to exchange-correlation potential of Perdew et al. [16] has been used. Concerning the relativistic effects, core states are treated fully relativistically in WIEN2k. For the valence states, a scalar relativistic scheme is used which describes the main contraction or expansion of various orbitals due to the mass-velocity correction and a fully relativistic scheme with spin–orbit coupling included in a second variational treatment using the scalar-relativistic eigenfunctions as basis [15]. The sphere radii were chosen as 2.8 a.u. for Th, 1.8 a.u. for Zr, 2.5 a.u. for Sr and 1.55 a.u. for O. The plane-wave cutoff K_{cut} is determined by $R_{mt}K_{cut} = 9.0$. The Blöchl's modified tetrahedron

method [17] was employed for the DOS calculations. The oxygen Kα XES spectra were calculated using Fermi's golden rule and the matrix elements between the core and valence states (following the formalism of Neckel et al. [18]); as implemented in the WIEN2k code. The calculated spectra include broadening for the spectrometer and core and valence lifetimes.

3. Results and discussion

3.1. Elastic properties

The calculated equilibrium lattice constants (a_0) for cubic $SrThO_3$, $SrZrO_3$ as well as for ThO_2 are given in Table 1, and are in a reasonable accordance with the available data. For $SrThO_3$ the predicted a_0 is higher than a_0 ($SrZrO_3$) by ~9.2 %. This result can be easily explained by considering the radii of cations: $R(Zr^{4+}) = 0.072$ nm versus $R(Th^{4+}) = 0.092$ nm.

Next, we have obtained the elastic constants (C_{ij}) for cubic $SrThO_3$, $SrZrO_3$ and ThO_2. These three independent elastic constants in a cubic symmetry (C_{11}, C_{12} and C_{44}) are estimated by calculating the stress tensors on applying strains to an equilibrium structure. All these constants for cubic $SrThO_3$, $SrZrO_3$ or ThO_2 phases are positive and satisfy the generalized criteria (see [28]) for mechanically stable crystals: $(C_{11} - C_{12}) > 0$; $(C_{11} + 2C_{12}) > 0$; $C_{11} > 0$; $C_{44} > 0$, see Table 2. Comparison of the elastic constants computed for $SrThO_3$ and $SrZrO_3$ indicates that Sr thorate is less resistant to shear deformation and especially to compression since C_{11} and C_{44} are decreased at about 117.2 GPa and 43.7 GPa, respectively. For both materials C_{11} are lower than for thoria.

In the following step, we have calculated the main elastic parameters for cubic $SrThO_3$, $SrZrO_3$ and ThO_2 namely, bulk modulus (B), compressibility ($\beta = 1/B$), shear modulus (G), Young modulus (Y), Poisson ratio (v) and Lame constants (λ, μ). These elastic parameters are usually calculated by two approximations: due to Voigt (V) [29] and Reuss (R) [30], in the following forms: bulk modulus:

$$B_{V,R} = (C_{11} + 2C_{12})/3, \quad (1)$$

shear modulus:

$$G_V = (C_{11} - C_{12} + 3C_{44})/5;$$
$$G_R = 5(C_{11} - C_{12})C_{44}/\{4C_{44} + 3(C_{11} - 3C_{12})\}, \quad (2)$$

Note that these elastic moduli are estimated from first-principle calculations of $SrThO_3$, $SrZrO_3$ and ThO_2 monocrystals. However, these industrially used materials are polycrystals, therefore it is useful to estimate the corresponding parameters of the polycrystalline species from the elastic constants of the single crystals. To this aim we utilize the Voigt–Reuss–Hill (VRH) approximation (see [31–33]). In this approach, according to Hill [31], the Voigt and Reuss averages are limits and the actual effective moduli for polycrystals could be approximated by the arithmetic mean of these two bounds. In this way, when a bulk modulus (B_{VRH}) and a shear modulus (G_{VRH}) are obtained from the values of $B_{V,R}$, Eq. (1) and $G_{V,R}$, Eq. (2) by the VRH approach, one can calculate the averaged Young modulus (Y_{VRH}) by the expression:

$$Y_{VRH} = 9B_{VRH}/\{1 + (3B_{VRH}/G_{VRH})\}.$$

Then, from the B_{VRH}, G_{VRH} and Y_{VRH} values the Poisson's ratio (v) and Lame's constants (μ, λ) for polycrystalline $SrThO_3$, $SrZrO_3$ and ThO_2 were obtained as

$$v = (3B_{VRH} - 2G_{VRH})/2(3B_{VRH} + G_{VRH}),$$
$$\mu = Y_{VRH}/2(1 + v); \quad \lambda = vY_{VRH}/\{(1 + v)(1 - 2v)\}.$$

Table 2 gives our calculated values of the mentioned elastic parameters for $SrThO_3$, $SrZrO_3$ and ThO_2 in comparison with available experimental and theoretical data.

As it can be seen, the bulk modulus decreases going from $SrZrO_3$ to $SrThO_3$; this trend correlates with changes in the lattice constants i.e. when the lattice constant increases by replacing Zr^{4+} with the larger Th^{4+} cation. This simple trend – when a larger lattice constant leads to a smaller bulk modulus – has been demonstrated also for different perovskites ABO_3 [42]. The compressibility (β) decreases (from

Table 1
Equilibrium lattice parameters (a, in nm) for thoria and cubic phases $SrThO_3$, $SrZrO_3$ according to our FLAPW calculations in comparison with available data

Phase	a[a]
$SrThO_3$	0.45426 (0.443 [8][b])
$SrZrO_3$	0.41578 (0.4154 [19]; 0.4109 [20]; 0.417 [21])
ThO_2	0.56225 (0.55969 [22]; 0.56001 [23]; 0.55976 [24]; 0.5535 [25]; 0.5595 [26]; 0.561 [27])

[a] The available experimental and calculated data are presented in parentheses.

[b] In assumption of pseudo-monoclinic unit cell with $a = b = c$ and $\beta = 90°$.

Table 2
Calculated elastic constants (C_{ij}, in GPa), bulk modulus (B_0, in GPa), compressibility ($\beta = 1/B_0$, in GPa^{-1}), shear modulus (G, in GPa), Young's modulus (Y, in GPa), Poisson's ratio (v) and Lame's constants (λ, μ) for cubic $SrThO_3$, $SrZrO_3$ and ThO_2

Parameters[a,b]	$SrThO_3$	$SrZrO_3$	ThO_2
Elastic constants			
C_{11}	197.3	368.1 (355 [27])	314.5 (338.6 [21])
C_{12}	67.1	105.2 (106 [27])	73.1 (71 [21])
C_{44}	31.9	75.6 (54 [27])	75.7 (77 [21])
Bulk modulus (V, R, VRH)	110.5	153.6; (160 [21]; 171 [34]; 150 [35])	192.8; (189 [27]; 223 [37]; 262 [26]; 195 [22]; 290 [25]; 175 [38]; 221 [39]; 193 [36])
Compressibility (VRH)	0.00905	0.00651	0.00519
Shear modulus	45.2 (V); 40.1 (R); 42.7 (VRH)	93.7 (V); 88.9 (R); 91.3 (VRH); (100 [21]; 98.5 [41])	98.0 (V); 91.1 (R); 94.5 (VRH); (82 [27]; 106 [40])
Young's modulus (VRH)	113.4	226.6 (248 [21]; 269 [41])	243.7 (215 [27]; 261 [40][c])
Poisson's ratio (VRH)	0.329	0.252	0.289 (0.284–0.297 [40])[c]
Lame's constants (VRH)			
λ	82.1	129.8	92.7
μ	42.7	94.5	91.3

[a] The available data are presented in parentheses.
[b] The single-crystal values of search modulus according to Voigt (V) and Reuss (R) approximations are included; for polycrystalline materials according to Voigt–Reuss–Hill (VRH) approximation.
[c] For polycrystalline samples with various defects (impurities) and porosity.

$SrThO_3$ to $SrZrO_3$) as the size of the cation decreases. Since strong correlation between bulk modulus and hardness of materials has been confirmed in several papers (see, for example, review [43]), we expect from our calculated data that $SrThO_3$ should exhibit a lower hardness than $SrZrO_3$, whereas the material with the highest hardness will be ThO_2. This conclusion coincides with the behavior of the shear modulus G. Indeed, the hardness of a material is defined as its resistance to another material penetrating its surface, and this resistance is determined by the mobility of dislocations. Thus, one of the determining factors of hardness is the response of interatomic bonds to shear strain [44]. In our case, the shear modulus lowered in the sequence $ThO_2 > SrThO_3 > SrThO_3$, see Table 2, i.e. $SrThO_3$ has a minimal bond-restoring energy under elastic shear strain.

As shown in Table 2, Young modulus has the minimum value for $SrThO_3$. It is evident that in the cubic symmetry the Young's modulus is lowered by making $C_{11} - C_{12}$ and C_{44} smaller. These values are 241.4 GPa and 75.7 GPa for $SrZrO_3$ as compared with 130.2 GPa and 31.9 GPa for $SrThO_3$. In other words, for the perovskite-type oxides a rapid decrease of the Young modulus occurs with growing of their lattice constant.

The values of the Poisson ratio (v) for covalent materials are small ($v = 0.1$), whereas for ionic materials a typical value of v is 0.25 [43]. In our case the values of v for $SrZrO_3$ and $SrThO_3$ are at about 0.19 and 0.25, respectively, i.e. a higher covalent contribution in intra-atomic bonding for $SrZrO_3$ should be assumed, see also below. Besides, for covalent and ionic materials, the typical relations between bulk- and shear modulus are: $G \approx 1.1B$ and $G \approx 0.6B$, respectively. For our perovskites the calculated values of G_{VRH}/B_{VRH} are $0.77(SrZrO_3) > 0.60(SrThO_3)$, indicating that the covalent bonding is suitable for $SrZrO_3$.

3.2. Phase stability

To define the comparative stability of the perovskite-like $SrZrO_3$ and $SrThO_3$ phases, we have calculated the total energy difference ΔE_{tot} between $SrMO_3$ (where M are Zr or Th) and a mixture of the constituent oxides as

$$\Delta E_{tot} = E_{tot}(SrMO_3) - \{E_{tot}(MO_2) + E_{tot}(SrO)\}. \quad (3)$$

In Eq. (3), E_{tot} are the total energies at the optimized geometries which correspond to the free energies of cubic $SrMO_3$, ThO_2, the ground state phase of zirconia (monoclinic ZrO_2) and cubic

SrO at p, $T = 0$ conditions, and we can consider ΔE_{tot} *as estimations of the stability of* $SrMO_3$ *phases.*

In this way, we have obtained ΔE_{tot} values: −0.507 eV/(formula unit) and +1.440 eV/(formula unit) for cubic phases $SrZrO_3$ and $SrThO_3$, respectively. Thus, our results show that at zero temperature and zero pressure $SrZrO_3$ has the negative, whereas $SrThO_3$ – the positive energy, i.e. the formation of $SrZrO_3$ is favorable. Moreover, in our calculations of the ground state phase of $SrZrO_3$ with orthorhombic (s.g. 62) lattice we have obtained $\Delta E_{tot} = -0.735$ eV/(formula unit) – in agreement with the experimental [19] and theoretical [45] sequence of the $SrZrO_3$ phases: the most stable is the orthorhombic phase, whereas the cubic phase is the high-temperature polymorph.

On the contrary, cubic $SrThO_3$ is unstable in comparison with a mechanical mixture of the constituent binary oxides. Naturally other thermodynamic factors such as temperature and pressure will also play a role. Additionally, the stabilizing of Sr thorate may be caused by the distortion of the simple cubic structure to the more complex monoclinic phase.

3.3. Electronic properties

The electronic bands and densities of states (DOS) for cubic $SrThO_3$ in comparison with ThO_2 and $SrZrO_3$ are shown in Figs. 1 and 2 and some band structure parameters are listed in Table 3.

For ThO_2, the lower bands which are located between −21.6 and −16.8 eV and between −14.9 and −8.3 eV below the Fermi level (E_F), are predominantly of O 2s and Th 6p types, respectively. The upper valence band (VB) with the width of about 5.8 eV is derived mainly from O 2p orbitals with some admixture of Th states. Note, that there are appreciable contributions from Th 6d states in this energy range due to Th–O hybridization indicating the presence of a covalent bonding. Additionally, the Th 5f states bring some contribution to the occupied near-Fermi region, Fig. 2. The bottom of the conduction band (CB) is composed mainly of Th 6d, 5f states, and at higher energies the antibonding O 2p-like bands are placed. These results are in reasonable agreement with other work devoted to the ThO_2 electronic structure [27,46].

Let us discuss the electronic properties of $SrThO_3$. Here, it can be clearly distinguished between three separate valence bands. Two of them are located between −18.1 and −16.1 eV and between −14.9 and −11.8 eV below the Fermi level and are of (O 2s + Sr 4p) and Th 6p type, respectively. The highest valence band is placed from −3.85 eV up to the Fermi level and is composed mainly of O 2p orbitals. The band gap (BG) for $SrThO_3$ is found at about 2.25 eV. This BG is approximately twice smaller, as compared with ThO_2 (BG ≈ 4.60 eV). The bottom of the conduction band for $SrThO_3$ consists of the Th 5f orbitals, followed by the bands with Th 6d character. From the DOS picture for $SrThO_3$ appears that the covalent bonds in the crystal are due to the mixing of oxygen 2p orbitals with thorium 6d and 5f orbitals, whereas in this energy region the occupied Sr states are practically absent, i.e. strontium atoms in $SrThO_3$ lattice are presented as Sr^{2+} ions. We notice also the presence of Th 6p and O

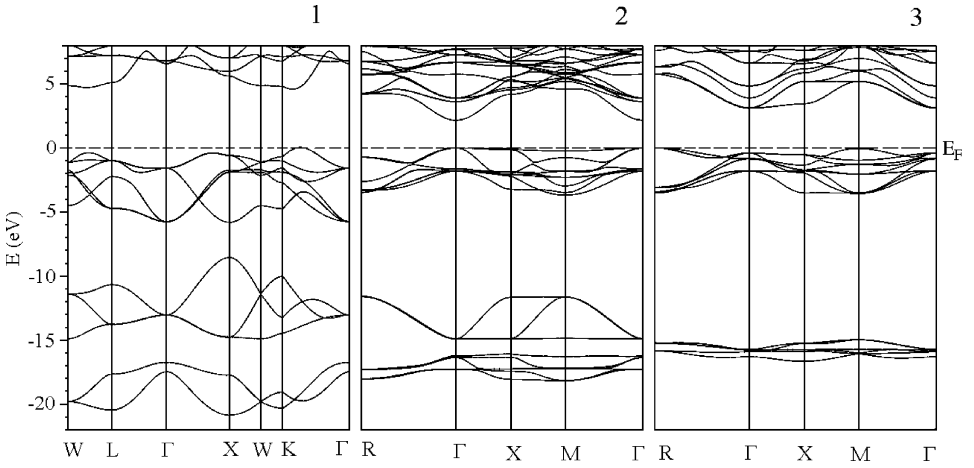

Fig. 1. Electronic bands for ThO_2 (1), $SrThO_3$ (2) and $SrZrO_3$ (3).

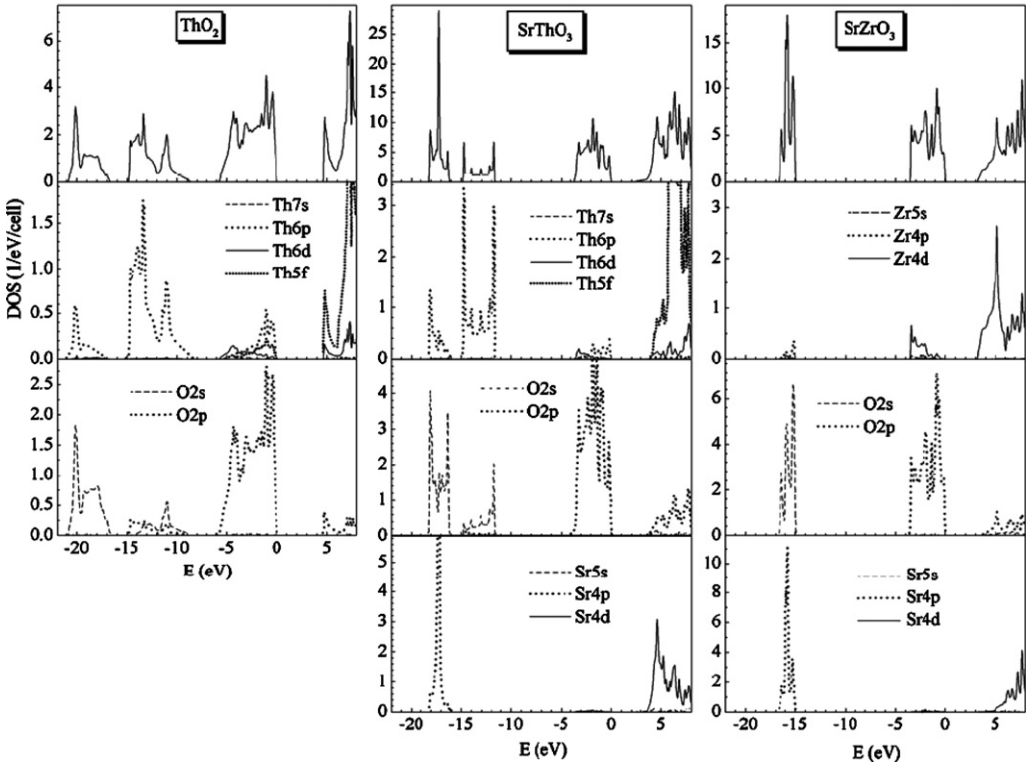

Fig. 2. Total (*upper panels*) and *l*-projected DOS for ThO_2, $SrThO_3$ and $SrZrO_3$. Fermi level $E_F = 0$ eV.

Table 3
The calculated minimal gaps (direct and indirect transitions, in eV) and occupied O 2p-like bands widths (eV) for cubic ThO_2, $SrThO_3$ and $SrZrO_3$ according to our FLAPW calculations

Phase	Minimal gaps[a]	Transition	Occupied O 2p bands width
$SrThO_3$	2.25	Direct (Γ)	3.85
$SrZrO_3$	3.20 (3.34[d]; 3.34[e]; 3.23[f]) 3.75 (3.62[e]; 3.50[f])	Indirect (R → Γ) Direct (Γ)	3.45 (3.7[d]; 4.32[e]; ≈4[f])
ThO_2	4.60 4.92 (4.82[b]; ≈5[c])	Direct (K–Γ) Indirect (Γ–Δ → K–Γ)	5.82 (≈4.1[b]; 4.9[c])

[a] The available data are presented in parentheses.
[b] Calculated by FLAPW method, Ref. [27].
[c] Calculated by LMTO method, Ref. [46].
[d] Calculated by FLAPW method, Ref. [21].
[e] Calculated by pseudopotential method (ABINIT code) [34].
[f] Calculated by DFT LCAO method [45].

2s contributions to the O 2s- and Th 6p bands, respectively, and these orbitals may also participate in chemical bonding.

In general, a similar picture for the electronic spectrum and orbital hybridization effects were obtained also for cubic $SrZrO_3$, Figs. 1 and 2. For $SrZrO_3$ the lower bands of (O 2s + Sr 4p) types are located between −16.5 and −14.8 eV below E_F. The upper VB with the width of about 3.45 eV is derived mainly from the O 2p orbitals with some admixture of Zr states. The bottom of the CB is composed mainly of Zr 4d states, and at higher energies the O 2p and Sr 4d-like bands are placed. The valence total density of states (see Fig. 2) is originated predominantly by O 2p states, which is consistent with $SrZrO_3$ being a formal d^0 system

with Zr^{4+} oxidation state. Nevertheless, there are appreciable contributions from Zr 4d states in the occupied energy range due to Zr–O hybridization indicating the presence of a covalent bonding. These features of the band structure agree well with the previous calculations for $SrZrO_3$ [21,34,45].

Looking at the charge density distribution (Fig. 3, where the charge density (ρ) in the (1 1 0) plane of $SrThO_3$ and $SrZrO_3$ is depicted) it is possible to observe the bonding picture of both materials. Here we see the increase of the charge density along the (Zr, Th)–O bond direction indicating the formation of covalent metal–oxygen bonds; in contrast, the charge density contours of strontium preserve the spherical-like form corresponding to ionic Sr^{2+} state. Note, that the ρ value between Zr–O is higher than for Th–O; this fact demonstrates the weakening of Th–O bonds in comparison with Zr–O bonds; it seems plausible these factors are responsible for the lowering of $SrThO_3$ stability as compared to $SrZrO_3$.

Finally, the band gap values are the most important parameters for a number of applications of the perovskite-like systems, which belong to the wide-band-gap oxides. Meanwhile it is well known that first principles band structure methods using the local density approximation (LDA) and the related generalized approximation (GGA) lead to a typical underestimating of the band gap for insulating materials – at about 30–50%, see [47–50]. For example, according to our present FLAPW-GGA data for $SrZrO_3$ a value of BG = 3.20 eV (indirect $R \rightarrow \Gamma$ transition) agree well with results of other LDA calculations (Table 3) but differ considerably from the experimental gap which is about 5.9 eV [51].

An empirical standard correction requires a fitting of the LDA gap to an experimental value [52]. In our case, for ThO_2 a calculated BG is equal to 4.6 eV while the experimental gap is about 6.0 eV [53]. Thus, a multiplicative correction factor (1.3) gets the calculated BG for ThO_2 closer to the experimentally measured gap. In this way, taking into account this factor, it is possible to estimate the 'experimental' value of the cubic $SrThO_3$ gap, which is about 3 eV. Note that the estimated value from our FLAPW-GGA BG for $SrZrO_3$ is higher: 4.2 eV.

3.4. X-ray emission spectra

As it is known, the intensity (I) of the X-ray emission spectra in the dipole approximation is determined by the DOS and the matrix elements and can be written as

$$I(E, \mathbf{e}) \sim E^3 \Sigma |\langle \mathrm{f}|\mathbf{e}\cdot\mathbf{r}|\mathrm{i}\rangle|^2 (\delta E_\mathrm{f} + E - E_\mathrm{i}), \quad (4)$$

where $\langle$f| and |i$\rangle$ refer to the final and initial one-electron states, E_i and E_f are the corresponding energy eigenvalues of the states involved in the transition. In our case, oxygen Kα (2p $\rightarrow$ 1s transition) XES probe directly the distributions of the occupied oxygen 2p DOS.

Fig. 4 shows the XES O Kα spectral shape of $SrThO_3$ in comparison with those for ThO_2 as obtained from FLAPW-GGA calculations. The spectra are depicted by alignment to the Fermi level. It can be seen that the spectrum of $SrThO_3$ consists of two subbands a and b separated by gap ~11 eV; where the subband b arises from the admixture of O 2p states into (O 2s + Th 6p) band. Going from

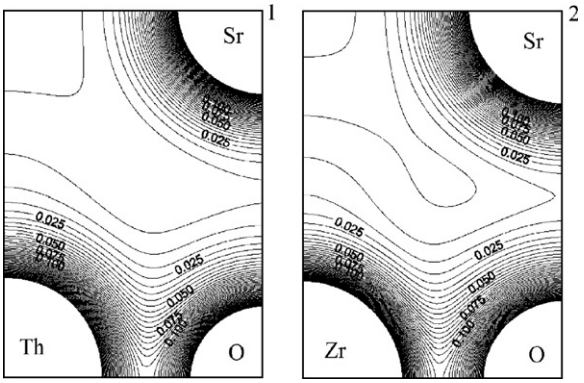

Fig. 3. Charge-density contour plots in (1 1 0) plane for $SrThO_3$ (1) and $SrZrO_3$ (2). The charge contours – in e/(a.u.)^3.

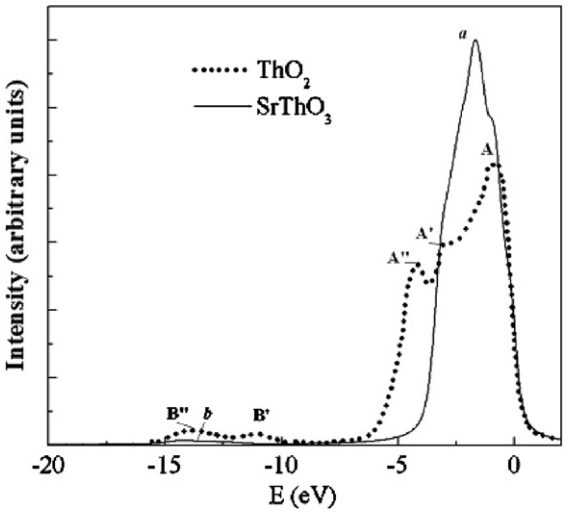

Fig. 4. Calculated O Kα X-ray emission spectra for ThO_2 and $SrThO_3$.

$SrThO_3$ to ThO_2, the O K spectral shapes change considerably. The main peak A for ThO_2 has broadened (at about 2 eV) with a pronounced substructure (additional peaks A′ and A″). The two low-lying peaks B′ and B″ appear in the region at about −14 to −12 eV below the Fermi level, originates from the O 2p states contribution to broad (O 2s + Th 6p) band. Thus, our data show that the O Kα XES of $SrThO_3$ differ drastically compared to ThO_2, i.e. the X-ray emission spectroscopy near the O Kα edge may be very useful technique for the phase analysis of complex ThO_2-based fuel materials.

4. Conclusions

In this work, the ab initio FLAPW-GGA method has been used for study of structural, elastic, cohesive and electronic properties of the meta-stable strontium thorate $SrThO_3$ in comparison with ThO_2 and $SrZrO_3$.

We have predicted the elastic constants for $SrThO_3$ and have discussed them in comparison with ThO_2 and $SrZrO_3$. We have utilized the Voigt–Reuss–Hill approximation to estimate the main elastic parameters (bulk modulus, compressibility, shear modulus, Young modulus, Poisson ratio, Lame constants) for polycrystalline $SrThO_3$, ThO_2 and $SrZrO_3$. We have found that cubic $SrThO_3$ should exhibit lower hardness than $SrZrO_3$, whereas the material with the highest hardness will be ThO_2.

Our first-principle calculations show that $SrThO_3$ has a positive energy of formation at zero temperature and zero pressure approximation – with respect to ThO_2 and SrO i.e. the cubic phase is unstable in comparison with a mechanical mixture of the constituent binary oxides. The calculated energies of formation for $SrZrO_3$ and $SrThO_3$ predict a higher lattice stability for $SrZrO_3$; this fact can be explained by considering the weakening of the covalent Th–O bond strengths as compared with Zr–O bonds. The Th–O bondings in $SrThO_3$ are due to the mixing of oxygen 2p orbitals with thorium 6d and 5f orbitals. In addition, the Th 6p and O 2s orbitals may also participate in chemical bonding. The corrected LDA gap for $SrThO_3$ has been estimated at about 3 eV.

Our calculations show that the O K edge X-ray emission spectra are very different for $SrThO_3$ and ThO_2, i.e. the XES technique may be very useful for detailed characterization of the stable and meta-stable ThO_2-based fuel materials.

Finally, the present discussion is focused on cubic $SrThO_3$ in comparison with $SrZrO_3$ and ThO_2. It would be of a great interest to examine the temperature effects on the comparative stability of $SrThO_3$ cubic versus monoclinic polymorphs – for example with using the recently developed thermodynamic approach based on first principle calculations [54]. Also to have more insight on the nature of the Th – containing ternary oxides, the further calculations of the structural, cohesive, elastic and electronic properties of the related compounds ($MThO_3$ and M_2ThO_3, where M = K, Na, Rb, Cs, Ca and Ba, see [3]) will be very useful.

Acknowledgement

This work was supported by the Russian Foundation for Basic Research, Grant No. 06-08-00808.

References

[1] R.D. Purohit, A.K. Tyagi, M.D. Mathews, S. Saha, J. Nucl. Mater. 280 (2000) 51.
[2] M. Ali (Basu), R. Mishra, S.R. Bharadwaj, A.S. Kerkar, S.D. Dharwadkar, D. Das, J. Nucl. Mater. 299 (2003) 165.
[3] S. Dash, Z. Singh, S.C. Parida, V. Venugopal, J. Alloys Compd. 398 (2005) 219.
[4] R. Prasad, S. Dash, S.C. Parida, Z. Singh, V. Venugopal, J. Nucl. Mater. 312 (2003) 1.
[5] R. Subasri, C. Mallika, T. Mathews, V.S. Sastry, O.M. Sreedharan, J. Nucl. Mater. 312 (2003) 249.
[6] H. Iwahara, in: Ph. Colomban (Ed.), Proton Conductors, Cambridge Univ. Press, Cambridge, 1992, p. 122.
[7] I. Mary-Szabo, Publ. Univ. Tech. Sci. Budapest, 1, 1947, 30.
[8] PC-PDF data, JCPDS-ICDD, 4-592, 1990.
[9] L.R. Goodenough, J.M. LangoLandolt–Bo˝rnstein Tables, Group III, vol. 4a, Springer, Berlin, 1970, p. 47.
[10] I. Solovyev, N. Hamada, K. Terakura, Phys. Rev. B 53 (1996) 7158.
[11] S.F. Matar, Progr. Solid State Chem. 31 (2003) 239.
[12] H. Iwahara, T. Yajima, T. Hibino, H. Ushida, J. Electrochem. Soc. 140 (1993) 1687.
[13] N. Kurita, N. Fukatsu, T. Ohashi, J. Jpn. Inst. Met. 58 (1994) 782.
[14] T. Yajima, K. Koide, H. Takai, N. Fukatsu, H. Iwahara, Solid State Ionics 79 (1995) 333.
[15] P. Blaha, K. Schwarz, G.K.H. Madsen, D. Kvasnicka, J. Luitz, in: K. Schwarz (Ed.), WIEN2K, An Augmented Plane Wave Plus Local Orbitals Program for Calculating Crystal Properties, Techn. Universität Wien, Austria, 2001.
[16] J.P. Perdew, S. Burke, M. Ernzerhof, Phys. Rev. Lett. 77 (1996) 3865.
[17] P.E. Blöchl, O. Jepsen, O.K. Andersen, Phys. Rev. B 49 (1994) 16223.
[18] A. Neckel, K. Schwarz, R. Eibler, P. Rastl, Microchim. Acta (Suppl 6) (1975) 257.

[19] B.J. Kennedy, C.J. Howard, B.C. Chakoumakos, Phys. Rev. B 59 (1999) 4023.
[20] A.J. Smith, A.J.E. Welch, Acta Crystallogr. 13 (1960) 653.
[21] R. Terki, H. Feraoun, G. Bertrand, H. Aourag, Phys. Status Solidi B 242 (2005) 1054.
[22] J.S. Olsen, L. Gerward, V. Kanchana, G. Vaitheeswaran, J. Alloys Compd. 381 (2004) 37.
[23] M. Idiri, T. Le Bihan, S. Heathman, J. Rebizant, Phys. Rev. B 70 (2004), art. 014113.
[24] U. Benedict, J. Less Common Met. 128 (1987) 7.
[25] P.J. Kelly, M.S.S. Brooks, J. Chem. Soc., Faraday Trans. II 83 (1987) 1189.
[26] J.-P. Dancausse, E. Gering, S. Heathman, U. Benedict, High Press. Res. 2 (1990) 381.
[27] R. Terki, H. Feraoun, G. Bertrand, H. Aourag, Comput. Mater. Sci. 33 (2005) 44.
[28] J. Wang, S. Yip, S.R. Phillpot, D. Wolf, Phys. Rev. Lett. 71 (1993) 4182.
[29] W. Voigt, Lehrbuch der Kristallphysik, Teubner, Leipzig, 1928.
[30] A. Reuss, Z. Angew. Math. Mech. 9 (1929) 49.
[31] R. Hill, Proc. Phys. Soc. London A 65 (1952) 349.
[32] D.H. Chung, Philos. Mag. 8 (1963) 833.
[33] G. Grimvall, Thermophysical Properties of Materials, North-Holland, Amsterdam, 1986.
[34] E. Mete, R. Shaltaf, S. Ellialtioglu, Phys. Rev. B 68 (2003) 035119.
[35] D. de Ligny, P. Richet, Phys. Rev. B 53 (1996) 3013.
[36] P.M. Macedo, W. Capps, J.B. Wachtman, J. Am. Ceram. Soc. 47 (1964) 651.
[37] K. Clausen, W. Hayes, J.E. Macdonald, R. Osborn, P.G. Schnabel, M.T. Hutchings, A. Magerl, Faraday Trans. II 83 (1987) 1109.
[38] J.H. Harding, P.J.D. Lindan, N.C. Pyper, J. Phys. C 6 (1994) 6485.
[39] S. Li, R. Ahuja, B. Johansson, High Press. Res. 22 (2002) 471.
[40] C. Keller, Thorium, Teil 2. Ternäre and polynäre Oxide des Thoriums. Gmelin Handbuch der Anorganischen Chemie, Springer, Heidelberg, Berlin, New York, 1976.
[41] S. Yamanaka, K. Kurosaki, T. Maekawa, T. Matsuda, S. Kobayashi, M. Uno, J. Nucl. Mater. 344 (2005) 61.
[42] R.D. King-Smith, D. Vanderbilt, Phys. Rev. B 49 (1994) 5828.
[43] J. Haines, J.M. Leger, G. Bocquillon, Ann. Rev. Mater. Res. 31 (2001) 1.
[44] S.-H. Jhi, J. Ihm, S.G. Louie, M.L. Cohen, Nature (London) 399 (1999) 132.
[45] R.A. Evarestov, A.V. Bandura, V.E. Alexandrov, E.A. Kotomin, Phys. Status Solidi B 242 (2005) R11.
[46] W.P. Ellis, A.M. Boring, J.W. Allen, L.E. Cox, R.D. Cowan, B.B. Pate, A.J. Arko, I. Lindau, Solid State Commun. 72 (1989) 725.
[47] L.J. Sham, M. Schluter, Phys. Rev. Lett. 51 (1983) 1888.
[48] J. Robertson, J. Vac. Sci. Technol. B18 (2000) 1785.
[49] P.W. Peacock, J. Robertson, J. Appl. Phys. 92 (2002) 4712.
[50] J. Robertson, K. Xiong, S.J. Clark, Thin Solid Films 496 (2006) 1.
[51] Y.S. Lee, J.S. Lee, T.W. Noh, D.Y. Byun, K.S. Yoo, K. Yamaura, E. Takayama-Muromachi, Phys. Rev. B 67 (2003) 113101.
[52] S. Tang, R. Wallace, A. Seabaugh, D. King-Smith, Appl. Surf. Sci. 135 (1998) 137.
[53] B.W. Veal, D.J. Lam, Phys. Rev. B 10 (1974) 4902.
[54] D. Fuks, S. Dorfman, S. Piskunov, E.A. Kotomin, Phys. Rev. B 71 (2005) 014111.